Extraction of Nonlinear Synergies for Proportional and Simultaneous Estimation of Finger Kinematics

Extraction of Nonlinear Synergies for Proportional and Simultaneous Estimation of Finger Kinematics.

Sanjay Kumar Dwivedi[1], Jimson Ngeo[2], *Member, IEEE,* and Tomohiro Shibata[1], *Member, IEEE.*

***Abstract*—*Objective*: Proportional and simultaneous estimation of finger kinematics from surface EMG based on the assumption that there exists a correlation between muscle activations and finger kinematics in low dimensional space. *Methods*: We employ Manifold Relevance Determination (MRD), a multi-view learning model with a nonparametric Bayesian approach, to extract the nonlinear muscle and kinematics synergies and the relationship between them by studying muscle activations (input-space) together with the finger kinematics (output-space). *Results*: This study finds that there exist muscle synergies which are associated with kinematic synergies. The acquired nonlinear synergies and the association between them has further been utilized for the estimation of finger kinematics from muscle activation inputs, and the proposed approach has outperformed other commonly used linear and nonlinear regression approaches with an average correlation coefficient of 0.91±0.03. *Conclusion*: There exists an association between muscle and kinematic synergies which can be used for the proportional and simultaneous estimation of finger kinematics from the muscle activation inputs. *Significance*: The findings of this study not only presents a viable approach for accurate and intuitive myoelectric control but also provides a new perspective on the muscle synergies in the motor control community.**

***Index Terms*—Muscle synergies, kinematic synergies, manifold relevance determination (MRD), proportional and simultaneous myoelectric control.**

I. Introduction

WITH the number of active controllable joints in robotic hands and powered prostheses substantially increasing every year, the capability to perform complex movements involving simultaneous control of a large degree-of-freedom (DOF) available in the hand is possible [1]. This makes it possible for the robot devices to generate human-like dexterous manipulation and replicate biomechanically realistic hand movement. Among many potential options, muscle interfacing using surface electromyographic (sEMG) signals is still currently the only viable noninvasive biological signal that can be used to control assistive devices for neurorehabilitation [2], such as active prostheses, or accomplish seamless myoelectric control of many applications.

There are many dexterous robotic hands and hand-prostheses but the difficulty in controlling all available degree-of-freedom (DOF) via myoelectric control has motivated many researchers to focus on more limited control mechanisms. Clinically available EMG-based controllers are only able to control a few DOF at a time [1]. Multiple dimensions have to be controlled sequentially, requiring slow mode-switching mechanisms initiated by different muscle co-contraction. As a result, significant research has been done on pattern recognition-based techniques to output multiple classes of movements, with many studies reaching decoding accuracies of above 95% and classifying up to more than six different hand gestures [3], [4]. Although in these approaches, the number of output movements is still limited and do not provide control of multiple correlated DOFs available in the hand. Current proportional myoelectric control strategies fall short in only being able to control a few number of DOFs [5], [6], among other existing limitations listed in [2]. Deployment of proportional and simultaneous control for multiple DOFs remains one of the major challenges in improving the next-generation myoelectric prostheses and interfaces [7].

Mapping of fine finger kinematic information from sEMG inputs has been done by numerous studies. However, dexterous hand manipulation remains to be one of the most complex biological movements to replicate [8], [9]. This is because the human hand not only has a highly articulated system, with possibly more than 20 kinematic DOF, but also has a complex muscular system involved in the motor control. Indeed a large part of the brain is shown to be devoted to controlling the hand's complex musculo-tendon network [8].

In neurophysiology, it has been argued that synergies control the coordination of muscle recruitment for posture control [10]. The muscle synergy hypothesis claims that the motor system directly initiates movement through flexible combinations of control modules recruited by the central nervous system to simplify control. Similarly, the concept of synergies has also been widely used in the field of robotics, where robot control laws are expressed in low-dimensional space to drive forces applied to the higher dimensional robot space. In motion planning, for example, synergies can often reduce complexity, where searching for an adequate kinematic configuration can increase exponentially with the dimensionality of the structure [11]. Thus, synergies can provide a natural modeling paradigm where muscle activation inputs and high-dimensional joint kinematics can be represented in low-dimensional space, where common latent features are shared. Estimating finger kinematics from sEMG input signals usually involves highly correlated patterns and high dimensionality in both the input and output domains. Nevertheless, few studies have given attention in considering such correlations in doing proportional and simultaneous control of the high dimensional finger kinematics from sEMG signals.

The present study aims at proportional and simultaneous estimation of finger kinematics from surface EMG by learning the nonlinear muscle and kinematic synergies and the asso-

[1]Kyushu Institute of Technology, Japan (email: dwivedi-sanjay-kumar@edu.brain.kyutech.ac.jp, tom@brain.kyutech.ac.jp).

[2]Skydisc Inc., Japan (email: jimsonngeo@gmail.com).

ciation between them. The main contributions of this study are as follows: 1) we propose a new strategy to extract the relationship between the muscle activations and the corresponding finger kinematics, using the Manifold Relevance Determination (MRD) [12], a generative, multi-view learning model coupled with a nonlinear dimension reduction method. 2) We present the thorough analysis of the nonlinear muscle and kinematic synergies (the shared latent space) extracted using the MRD model from the combined study of muscle activations (input-space) together with the finger kinematics (output-space). 3) Finally, we present the use of the acquired nonlinear synergies and their association (the shared latent space) to estimate the finger kinematics of a full 23-joint skeletal hand model. We provide an experimental evaluation that shows how the proposed method outperforms commonly used linear and nonlinear regression approaches, in terms of estimating finger kinematics using muscle activation inputs.

The rest of the paper is organized as follows. Section II introduces work related to muscle and kinematic synergies and their applications in myoelectric control. In Section III, the proposed framework for extracting the nonlinear muscle and kinematic synergies is discussed. Section IV and Section V describe the data set and the results obtained from the MRD model. Section VI discusses the advantages and limitation of this work. Finally, we conclude in Section VII with some future directions.

II. Related Work

This study is inspired by studies in the motor control community that claims that synergistic patterns can be observed in the muscle coordination and posture space. Grinyagin et al. [13] presented different types of synergies. First, static postural synergies, that refer to correlated models between single kinematic poses. Second, kinematic synergies, that consider time-dependent correlation during a motor action task [14]. Lastly, muscle synergies that uses recruited muscle coordination patterns from electromyographic (sEMG) activity to address low-level representations of motor control [15]–[17]. While only the third type of synergy has been largely used in the motor control community, the first two types have inspired a lot of work in robotics [11].

The use of muscle synergy model together with regression-based methods for robust myoelectric control has inspired a lot of work [5], [18]–[23]. Studies have shown that muscle synergy features are inherently robust to single channel electrode shift and amplitude cancellation [6], [24].

For better understanding of muscle synergies and their functional role, input spaces such as sEMG or EEG should be studied simultaneously with output spaces such as Kinematics or Force, etc. [25] and studies [26] [27] in the past have also focused in this direction by extracting the components using Nonnegative Matrix Factorization (NMF) from a dataset containing sEMG and task-related variables. However, the use of NMF to study a dataset obtained from the concatenation of muscle activations and task related variables, is not well justified due to the following three reasons.

First, NMF is a linear decomposition algorithm that may not be able to handle the nonlinearity that exists in sEMG and the corresponding task-related variables. Romero et al. [11] have shown that the postural synergies extracted using linear models failed to represent nonlinear motions even in a simple hand reaching and grasping tasks. Martin et al. [28] have shown that how synergies extracted using linear models failed to extract the agonist-antagonist relationships while synergies extracted using nonlinear models like auto-encoders can represent such information, successfully.

Second, non-negative constraint in the NMF is suitable for extracting positive coefficients from the muscle activations and giving a physiological interpretation to the extracted components and coefficients but not an appropriate choice for studying the task related variables which may also have negative values [25].

Third, the number of synergy components chosen are based on the reconstruction accuracy, in terms of the Variance Accounted For (VAF) or the Pearson Correlation Coefficient (ρ), which are only valid to a certain extent due to the noisy fluctuation in the biological data, instead of capturing task-specific variations in the muscle activity [29].

A study by Tagliabue et. al. [17] have shown that kinematic synergies have their origin in muscle synergy at least partially, first by extracting kinematic and muscle synergies, by applying PCA on each data separately, and then comparing the synergy vectors of same importance from two different spaces. However, just by using similarities, it is still premature to conclude that kinematic synergies have indeed their origins from muscle synergies, or is it the other way around. One can also hypothesize that muscle synergies have their origins from kinematic synergies instead, where it is assumed that the first-hand synergy, the 'palmar grasp reflex' is found at birth and later new muscle synergies are developed with growth [30].

Muscle activations and the generated movements are highly related and cannot be ignored, and to understand the relationship between these two (sEMG and finger kinematics) related but different observation spaces, a multi-view, nonlinear algorithm is better suited to handle this problem setting. In this direction, Ngeo. et al. [31] have shown the use of standard shared Gaussian Process Latent Variable Model (GPLVM) to study sEMG and finger kinematics together, however, GPLVM itself and all of its extensions, rely on a maximum a posteriori (MAP) training procedure which does not allow the Automatic Relevance Determination (ARD) procedure to take place to find the optimal number of latent dimension and makes the GPLVM models sensitive to overfitting [32].

In this study, we propose to use the MRD model to find the relationship between sEMG and finger kinematics. The MRD model is the extension of Bayesian Gaussian Process Latent Variable Model (BGPLVM) which allows for the automatic estimation of dimensionality of the latent space, and provides an approximation to the full posterior of the latent points given the data, making it robust to overfitting and data efficient approach [32].

III. Methods

In this section, we present the MRD model [12] and its formulation, used for finding the nonlinear muscle and kinematic

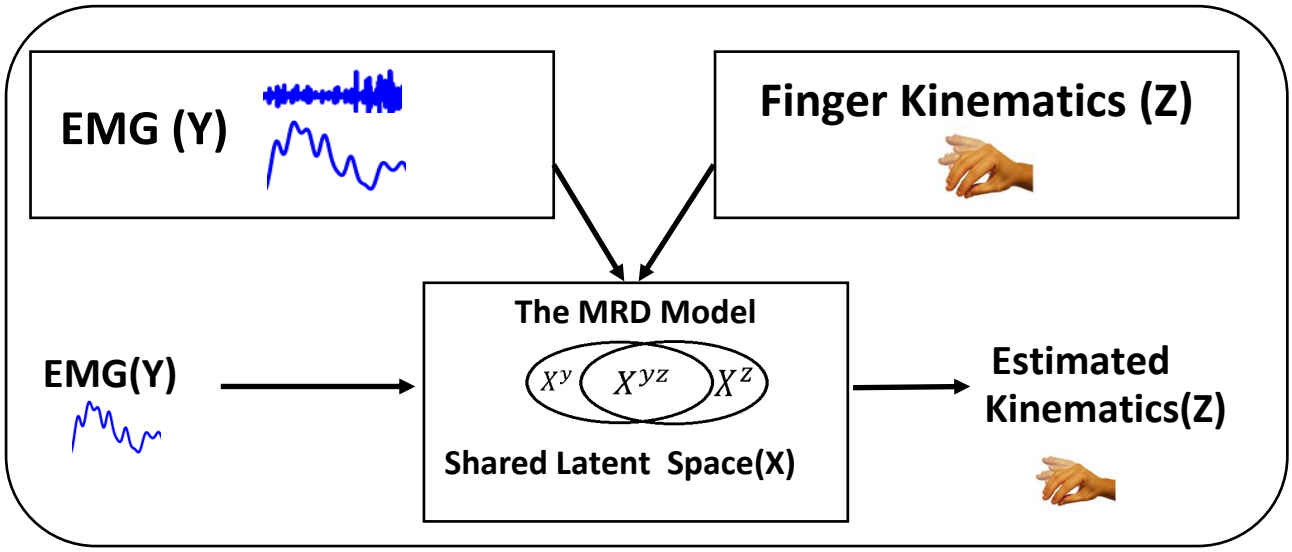

Fig. 1: Schematic overview of the proposed method for extracting the nonlinear muscle and kinematic synergies and their relationship, using the MRD model. Two different but related observation spaces, namely sEMG (Y), recorded from eight muscles in the forearm and the corresponding 3D coordinates of 23 joint marker positions in the hand (Z), which include three set of tasks, namely: (1) individual finger flexion-extension (IFFE), (2) all finger flexion-extension (AFFE), and (3) random flexion-extension of one or more fingers (RFFE), are given to the MRD model as input. The learned shared latent space (X) is comprised of three subspaces. First subspace (X^y) represents the independent muscle synergies, second subspace (X^{yz}) represents the association of muscle and kinematic synergies while the third subspace (X^z) which would represent the independent kinematic synergies, is rarely observed, in this study.

synergies and the interaction between them (shared latent space). First, the MRD model and its formulation is presented. The inference algorithm is then described, which is used to estimate finger kinematics from sEMG using the obtained shared latent space. Finally, the implementation details of the linear regression and artificial neural network are presented, which are later used in the study to compare the estimation performance of the MRD model.

A. Manifold Relevance Determination(MRD)

The problem is formulated as follows: Given that we have two observation data $Y \in \mathbb{R}^{N \times D_Y}$ and $Z \in \mathbb{R}^{N \times D_Z}$, the goal of the model is to find a factorized latent variable parameterization in a space $X \in \mathbb{R}^{N \times Q}$ that relates corresponding pairs of observations from different spaces Y and Z. It is assumed that the two datasets are generated from a low dimensional manifold mapped from smooth functions $\{f_d^Y\}_{d=1}^{D_Y} : X \to Y$ and $\{f_d^Z\}_{d=1}^{D_Z} : X \to Z$ $(Q << D)$, corrupted by noise:

$$y_{id} = f_d^Y(\mathbf{x}_i) + \epsilon_{id}^Y \tag{1}$$

$$z_{id} = f_d^Z(\mathbf{x}_i) + \epsilon_{id}^Z, \tag{2}$$

where $\{y, z\}_{id}$ represents dimension d of sample point i and ϵ_{id}^Y, ϵ_{id}^Z are sampled from a zero mean Gaussian distribution. This leads to the likelihood under the model, $P(Y, Z|X, \theta)$, where where $\theta = \{\theta^Y, \theta^Z\}$ contains the parameters of the mapping functions and noise variances. Finding the latent representation X and mapping functions f^Y and f^Z is an ill-constrained problem. Lawrence provided a solution by placing GP priors over the mapping and the resulting model is the Gaussian Process Latent Variable Model (GPLVM) framework [33]. In this framework, each generative mapping is modeled as a product of independent GP's parametrized by the kernel or covariance function $K = \{K^Y, K^Z\}$ evaluated over the latent variable X, so that

$$P(F^Y|X, \theta^Y) = \prod_{d=1}^{D_Y} \mathcal{N}(\mathrm{f}_d^Y|\mathbf{0}, K^Y), \tag{3}$$

where $F^Y = \{\mathrm{f}_d^Y\}_{d=1}^{D_Y}$ with $f_{id}^Y = f_d^Y(\mathbf{x}_i)$, and similarly for F^Z. This allows the general nonlinear mapping function F to be marginalized out leading to a likelihood function in the form of a product of Gaussian densities:

$$P(Y, Z|X, \theta) = \prod\nolimits_{\mathcal{K}=\{Y,Z\}} \int p(\mathcal{K}|F^{\mathcal{K}}) p(F^{\mathcal{K}}|X, \theta^{\mathcal{K}}) dF^{\mathcal{K}} \tag{4}$$

Integration over (4) is then done by variationally marginalizing out X by using variational approximation techniques used for standard GPLVMs. A non-standard but analytical solution through variational learning techniques and using induced variables is described in [12], [34], [35]. The shared latent space (X) is composed of three subspaces, representing the shared and private variance for each observation data, $X = \{X^Y, X^{YZ}, X^Z\}$. Bayesian training automatically allocates the dimension of this shared latent space (X) using automatic relevance determination (ARD) priors [12]. In the automatic allocation of the dimensionality, the dimensions D_Y and D_Z of the latent functions f^Y and f^Z, respectively, are

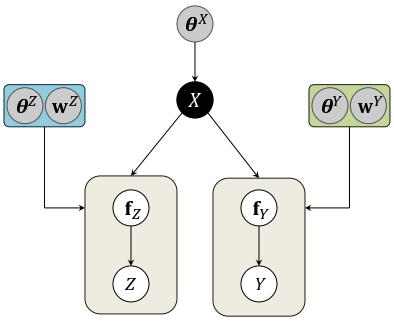

Fig. 2: Graphical model of the MRD model. A distribution for shared latent space X is learned and the hyperparameters $\mathbf{w}^{Y,Z}$ and $\theta^{Y,Z}$ are the ARD weights that determine the dimensionality and the function model parameters, respectively.

selected to be independent draws of a zero-mean GP with an ARD kernel or covariance function with the following form:

$$k^{\{Y,Z\}}(\mathbf{x}_i, \mathbf{x}_j) = (\sigma_{ard}^{\{Y,Z\}})^2 e^{-\frac{1}{2}\sum_{q=1}^{Q} w_q^{\{Y,Z\}}(x_{i,q}-x_{j,q})^2}. \quad (5)$$

where $w_q^{\{Y,Z\}} = \alpha(l_q^{\{Y,Z\}})^{-2}$, with α a constant positive scale value and length scales l. Although a common distribution for X is learned, two sets of ARD weights $W = \{\mathbf{w}^Y, \mathbf{w}^Z\}$ are obtained to automatically infer the relevance of each latent dimension for generating points in the Y and Z spaces respectively. The latent shared subspace $X^{YZ} \in \mathbb{R}^{N\times Q_S}$ is then defined by the set of dimensions $q \in [1, \cdots, Q]$ for which $w_q^Y, w_q^Z > \delta$, with δ close to zero and $Q_S \leq Q$. As for the two private spaces, X^Y and X^Z, these are also inferred automatically along with their corresponding dimensionalities, Q_Y and Q_Z, respectively. More specifically:

$$X^Y = \{\mathbf{x}_q\}_{q=1}^{Q_Y} : \mathbf{x}_q \in X, w_q^Y > \delta, w_q^Z < \delta. \quad (6)$$

and analogously for X^Z. This model is summarized in the graphical model shown in Fig. 2. The Bayesian GPLVM Matlab toolbox [36] was used to implement the model training and dimensionality relevance determination in this study.

1) Inference Algorithm: To predict finger kinematics from sEMG, the nearest neighbor approach (NN) to search for a similar point in the training data for the given sEMG was used, details of which explained in algorithm 1.

Algorithm 1 Inference of Finger Kinematics Z, given sEMG Y

1: *Given* : MRD model trained on two views (Y, Z)
2: *Given* : A test point y_*
3: Find y_{train} = *NN*(Y_{train}, y_*)
4: Select $x_*(x_*^y, x_*^{yz}, x_*^z)$ from $X(X^y, X^{yz}, X^z)$ corresponding to the index of y_{train}
5: Find $x_*^{ss} = NN(X^{yz}, x_*^{yz})$
6: Predict $z_* = P(Z|x_*^{ss})$

x_*^{ss} denotes a latent point closest to the x^* in the coupled latent dimensions.

B. Linear Regression (LR)

A simple linear regression has been performed between muscle activations and finger kinematics using the MATLAB "\" operator. Simple linear regression in the MATLAB considers only one independent variable (x) as :

$$y = mx + c + \epsilon \quad (7)$$

where y is the response variable, c is the y-intercept, m is the slope (or regression coefficient), and ϵ is the error term.

C. Artificial Neural Network (ANN)

ANN has been implemented using the fitnet function of MATLAB with default training algorithm Levenberg-Marquardt ('trainlm') from the Netlab toolbox. The network is made of an input layer, a hidden layer with a tan-sigmoidal activation function, and a single linear output layer. The number of neurons in the hidden layer is set to be the 2/3 of the sum of the neurons in the input and output layer. Parameters of the network were obtained by minimizing a mean square error function. A single network is used to simultaneously and continuously estimate the finger kinematics from the muscle activations.

D. Statistical Significance Test

A repeated measure one-way ANOVA is conducted separately for each of the three evaluation metrics, namely Correlation Coefficient, R-square and Root Mean Square Error (RMSE), respectively, to determine if the accuracy of estimated finger kinematics were significantly improved using MRD model when compared with other commonly used regression approaches. Lilliefors test has been used to ensure that the dependent variables follow the normal distribution. The level of significance is set to $p < 0.05$ for the main test, while post-hoc comparisons are performed using pair-wise t-test, and the p-value is corrected using the Bonferroni method.

IV. DATASETS

A. Data Collection

Surface EMG signals were extracted from eight extrinsic muscles of the hand that known to contribute to the wrist and finger movements (Fig. 3). Bipolar active-type Ag-AgCl electrodes, with an inter-electrode distance of 20 mm, were placed on the extrinsic muscles of the forearm. The target muscles and the related finger movements are listed in Table I. A single electrode was also placed on the subject's olecranon to serve as ground and reference electrode.

The sEMG signals were measured using a compact BA1104 pre-amplifier and a TU-4 telemetry unit (Digitex Lab. Co. Ltd). The obtained sEMG signals from the hardware were in the frequency range from 1 Hz to 1 kHz. The sEMG signals were sampled at 2 kHz, and were digitized by an A/D converter with 12-bit precision. The sEMG signals were displayed on a real-time monitor and visually inspected to check its quality. Along with the sEMG signals, unconstrained and continuous wrist and finger movements were also simultaneously recorded using a MAC3D motion capture system (Motion Analysis Corp.). Twenty-three passive reflective markers were attached on the subject's hand (see Fig. 3), one on each joint and tip of the finger, three in the wrist area and one in the forearm

for reference. The Cortex software from Motion Analysis was used to concurrently record and synchronize the sEMG and motion data. The marker positions were recorded at 200 Hz sampling rate with measurement units in millimeters (mm). The full hand kinematic dimension is given by the 23-marker hand skeleton model 3D information in the motion capture space. Later on, the metacarpophalangeal (MCP), the proximal interphalangeal (PIP) and the distal interphalangeal (DIP) joint angles were also calculated from the recorded marker positions following the procedure described in [38]. Because the thumb does not have a DIP joint, the carpometacarpal (CMC) joint was considered. These joint angle values are used in EMG-to-Muscle activation model.

The total data used included those of 10 healthy and intact participants (9 Male, 1 Female, aged 26-31 years old). An informed consent has been taken from every subject before the experiment following the principles of declaration of Helsinki. The subject, seated with their dominant hand and elbow comfortably positioned on a flat surface table, were asked to do different flexion and extension finger movement tasks which includes the following:

1) Individual finger flexion-extension (IFFE)
2) All finger flexion-extension (AFFE)
3) Random flexion-extension of one or more fingers (RFFE)

In the first task, the subject was asked to move one finger at a time, in the flexion-extension plane of each finger. The second task involved the subject moving all fingers simultaneously, in the same flexion-extension plane. This motion resembled the opening and semi-closing of the hand. Full closing of the hand was not possible as some markers at the tip of the fingers would not be seen by the motion capture system. In these first two tasks, the subjects mainly did MCP flexion and extension, in which the PIP and DIP followed the movements of the MCP joint. Finally, for the third and last part of the experiment, the subject was asked to move any finger freely in any direction within the motion capture volume space while still maintaining a fixed neutral position for the arm and elbow. Irregular movements and different finger combinations for flexion and extension movement were encouraged from the subject in this last part of the experiment. However, in this task fingers barely reached to maximum flexion or extension.

The first task consisted of 5 sets of movement, one for each finger. While the remaining tasks consisted of 1 set each. Each set consisted of 5 trials with each trial lasting 20 seconds. All the movements were limited to finger flexion and extension movements while the rest of the arm (e.g. wrist, elbow, etc.)

TABLE I: Selected sEMG Channels and the target muscles

C	Target Muscle	Hand/Finger
1	Abductor pollicis longus(APL)	Thumb abduction,extension
2	Flexor carpi radialis(FCR)	Wrist, hand flexion
3	Flexor digitorum superficialis(FDS)	2-5th finger PIP flexion
4	Flexor digitorum profundus(FDP)	2-5th finger DIP flexion
5	Extensor digitorium(ED)	2-5th finger extension
6	Extensor indices(EI)	Index finger
7	Extensor carpi ulnaris(ECU)	Wrist extension and abduction
8	Extensor carpi radialis(ECR)	Wrist and thumb

Source: Anatomy and Kinesiology of the Hand [37].

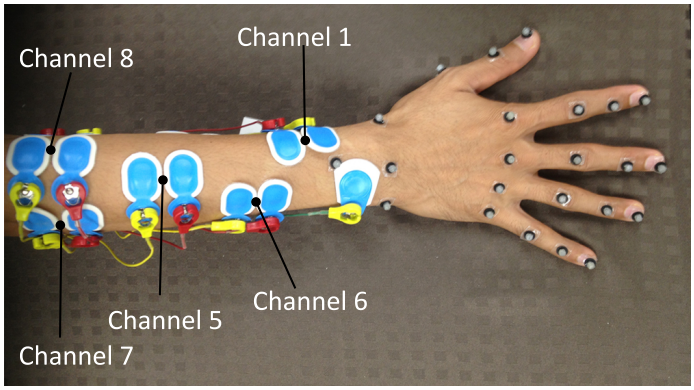

Fig. 3: Shows the placement of electrodes in the target muscles of the forearm as shown in the Table I and position of 23 markers in the hand.

maintained a fixed position upon instruction. Markers on the wrist joint were also recorded to ensure that the wrist maintained a fixed position, or at least minimal ulnar/radial angle deviation. A ringing sound, from the motion capture device, signaled the start and end of a trial in the experiment. All the trials were sequentially done and the participants were allowed to rest anytime throughout the experiment. The subjects could make as many movements but were instructed to move in their own perceived normal velocity ($\leq$ 2 cycles of movement per second) and to maintain the least amount of wrist ulnar/radial angle deviation. The subjects were tasked to reach maximum flexion and extension for each finger at least once at any point in any of the trials. The overall measured and normal range of finger joints has been shown in the Table II. There was no obstacle or object to impede/induce force in the experiment. A video demonstration (Recorded_Kine.mp4) of the recorded finger kinematics corresponding to all three tasks are provided in the supplementary material.

B. Data Preprocessing

1) EMG-to-Muscle activation model: The raw sEMG signals were first preprocessed into a form, that after further manipulation, can be used to estimate muscle activation [39], [40]. An EMG-to-Muscle Activation model is used to consider the effects of electromechanical delay (EMD) and activation dynamics in place of sEMG delay lines. It has been shown in previous studies, that using this feature works very well in estimating muscle force [41], finger kinematics [42], and finger force in an online myocontrol system [9].

The raw sEMG signals were digitally band-pass filtered in the range of [10, 500] Hz using a 4th-order Butterworth filter. The sEMG signals were then rectified, normalized by the overall peak rectified sEMG obtained, low-pass filtered (4 Hz cut-off frequency, zero-phase, 4th-order Butterworth filter) and downsampled to match the frequency of the motion data.

Buchanan et al. proposed a second-order model filter that works more efficiently to model the relationship between sEMG and muscle activation [39], [40]. In this study, we

TABLE II: Finger joints normal and measured range of motion.

Finger Joint	DOF	Type of Motion	Theoretical Range	Measured Range
Thumb CMC	1	Hyperextension/Flexion	−10/55 deg	$9.86 \pm 21.17/50.06 \pm 11.39$ deg
Thumb MCP	2	Hyperextension/Flexion	−10/55 deg	$-3.05 \pm 4.94/56.51 \pm 8.34$ deg
Thumb IP	3	Hyperextension/Flexion	−15/80 deg	$-4.52 \pm 8.40/57.27 \pm 18.01$ deg
Index MCP	4	Extension/Flexion	−45/90 deg	$-39.97 \pm 15.00/62.29 \pm 14.27$ deg
Index PIP	5	Extension/Flexion	0/100 deg	$-14.95 \pm 12.42/72.55 \pm 16.87$ deg
Index DIP	6	Extension/Flexion	0/80 deg	$-16.96 \pm 13.97/45.51 \pm 22.25$ deg
Middle MCP	7	Extension/Flexion	−45/90 deg	$-34.07 \pm 10.29/69.39 \pm 11.61$ deg
Middle PIP	8	Extension/Flexion	0/100 deg	$-16.87 \pm 12.88/80.07 \pm 16.52$ deg
Middle DIP	9	Extension/Flexion	0/80 deg	$-15.15 \pm 11.77/57.07 \pm 22.42$ deg
Ring MCP	10	Extension/Flexion	−45/90 deg	$-26.35 \pm 10.71/62.51 \pm 11.04$ deg
Ring PIP	11	Extension/Flexion	0/100 deg	$-15.34 \pm 11.44/88.58 \pm 14.21$ deg
Ring DIP	12	Extension/Flexion	0/80 deg	$-14.52 \pm 11.36/58.94 \pm 19.99$ deg
Little MCP	13	Extension/Flexion	−45/90 deg	$-14.31 \pm 12.59/69.27 \pm 6.07$ deg
Little PIP	14	Extension/Flexion	0/100 deg	$-14.66 \pm 12.59/72.94 \pm 14.27$ deg
Little DIP	15	Extension/Flexion	0/80 deg	$-10.09 \pm 8.45/84.54 \pm 12.60$ deg

employed such a filter to obtain muscle activation $v_j(t)$ given by:

$$u_j(t) = \alpha e_j(t-d) - \beta_1 u_j(t-1) - \beta_2 u_j(t-2) \quad (8)$$

$$v_j = \frac{e^{A_j u_j(t)} - 1}{e^{A_j} - 1} \quad (9)$$

where $e_j(t)$ is the rectified, normalized and filtered sEMG of muscle j at time t. In this model, α, β_1, β_2 are recursive coefficients of the filter, d is the EMD parameter and A handles the nonlinearity parameter of the activation feature. Filter stability is guaranteed by subjecting α, β_1, and β_2 to the following constraints:

$$\beta_1 = \gamma_1 + \gamma_2 \quad (10)$$

$$\beta_2 = \gamma_1 \cdot \gamma_2 \quad (11)$$

$$|\gamma_1| < 1, |\gamma_2| < 1 \quad (12)$$

$$\alpha - \beta_1 - \beta_2 = 1 \quad (13)$$

The muscle activation model parameters are obtained using a linear regressor and optimized through constrained nonlinear programming using the Matlab Optimization Toolbox by minimizing the following cost function:

$$\frac{1}{N} \sum_t (Z_{\text{ANGLE\_EST}} - Z_{\text{ANGLE\_TARGET}})^2 \quad (14)$$

where N is the total number of training samples, $Z_{\text{ANGLE\_TARGET}}$ are calculated from the measured joint marker positions [38] and, $Z_{\text{ANGLE\_EST}}$ are obtained by linear regression of muscle activation values as following:

$$Z_{\text{ANGLE\_EST}}(t) = w_0 + \sum_{i=1}^{15} \sum_{j=1}^{8} w_{ij} \cdot v_j(t) \quad (15)$$

The variable i refers to the 15 finger joint angles and j refers to the eight muscles in the expression (15). To convert processed sEMG (e_j) in to the muscle activations (v_j), the muscle activation parameters are first initialized manually (*i.e.* $\gamma_1 = -0.9782, \gamma_2 = -0.9782$, $d = 0.045$ and $A = -3$) following the recommendation given in [39] and satisfying the constraints (12) and (13), while linear regression parameters (*i.e* w_0, w_{ij}) are initialized by performing linear regression from processed sEMG (e_j) to $Z_{\text{ANGLE\_TARGET}}$.

Next, the constrained nonlinear programming (MATLAB function - 'fmincon' with 'active-set' algorithm) is used to find the best possible value of parameters (*i.e* $w_0, w_{ij}, \gamma_1, \gamma_2, d$ and A) by minimizing the cost function (14).

2) Finger Kinematics: The motion data, on the other hand, were also low-pass filtered (4 Hz cut-off frequency) to remove any jitters. In this study, a factorized latent representation X is extracted from the 8-channel muscle activation input $Y \in \mathbb{R}^{N\times 8}$ and from the 23-marker finger posture $Z \in \mathbb{R}^{N\times 69}$. We considered all the 3D information on each marker which summed up to a total of 69 dimensions in the hand kinematic space.

C. Training Data to the Models

All the models are separately trained for each subject and for a subject there are in total $140,000$ sample data points ($\mathbb{R}^{140{,}000\times 8}$ and $\mathbb{R}^{140{,}000\times 69}$ for muscle activations and finger kinematics, respectively) from three sets of tasks corresponding to all five trials.

1) MRD Model:

a) For Synergistic Analysis: Data points from all five trials of task 1 (IFFE) and task 2 (AFFE) combined together, shuffled and then further downsampled by a factor of 30. Downsampling is done because training the MRD model is computationally expensive for large datasets, but handles data with large dimensions very well. 70% of the downsampled dataset (around 2800 data points) is used as training data.

For Synergistic Analysis, task 3 (RFFE) have not been included in the model training as the motions were random across the trials and subjects, and may pose difficulties in the interpretation and comparison of the obtained synergy components in and across the subjects.

b) For Finger Kinematics Estimation: To check and compare the estimation capability of the nonlinear synergistic features obtained from the MRD model with other commonly used linear and nonlinear approaches, new sets of MRD models were trained for each subject, but now including the data from all three tasks, keeping rest of the training procedure same as used for synergistic analysis. Estimation performance is evaluated over the full dataset (around 136,000 data points) without down-sampling except for the data points which were used for training the MRD models.

2) Artificial Neural Network (ANN) and Linear Regression (LR) :

a) ANN and LR using Full Dimensions (ANN-FULL, LR-FULL) : Data points from all the five trials and three set of tasks were combined together, shuffled and then further down-sampled by a factor of 30. Similar to the MRD model, 70% of the down-sampled dataset is used as training data, while the full dataset (around 136,000 data points) excluding the training data points are used as the test data.

b) ANN and LR using Reduced Dimensions (ANN-RD, LR-RD) : As the MRD model makes use of reduced dimensions (shared latent space) to map data from one view into another, ANN and LR were also trained on reduced dimensions, extracted by applying Principle Component Analysis (PCA), separately, on each of the full datasets (All five trials, three sets of tasks) corresponding to the muscle activation and the finger kinematics, respectively. The number of reduced dimensions or principal components was selected based on 90% total accumulated data variance. Five and nine principal components were needed to explain 90% of the data variance in the sEMG and finger kinematics data, respectively. Following the similar training and test procedure, datasets of reduced dimensions were shuffled and down-sampled by a factor of 30, 70% of which is used as training data, while the full dataset (around 136,000 data points) excluding the training data points are used as the test data. Predicted data points were recovered back to the original space to evaluate the performance metrics.

For ANN and LR, the down-sampling of the dataset has been done to keep the number of training data points similar to that of the MRD model. Increasing the training samples [42], using the deep neural network architecture Or creating a dedicated MLP for each DOF [43] may lead to better estimation performance, but how large the training data is required or how deep the network architecture should be or to what extent retraining the model is needed, has not been investigated in this study.

As the focus of the study is to provide a data efficient approach to extract and interpret the nonlinear synergy components by studying sEMG (input space) together with the task-related variables (output space) and their application in estimating finger kinematics.

D. Performance Evaluation Metrics

The quality of estimated finger kinematics is evaluated using the three metrics namely root-mean-square error (RMSE), Correlation Coefficient (ρ) and R-square.

$$\text{RMSE}_i = \sqrt{\frac{\sum_{t=1}^{N}(Z_{\text{MEASURED}} - Z_{\text{EST}})^2}{N}} \tag{15}$$

where Z_{MEASURED} and Z_{EST} are the measured and estimated x, y and z coordinates of the 23 marker positions, respectively. The value of N would be 69. The RMSE performance index gives the square root of the mean of the square of all of the error. Compared to other error metrics, RMSE amplifies and severely punishes large errors. The other two performance metrics, correlation Coefficient (ρ) and R-square are also calculated between Z_{MEASURED} and Z_{EST}.

V. Results

A. Shared latent space obtained using the MRD model

To find the shared latent space (X) between the sEMG and the finger Kinematics, eight muscles activations and the corresponding 3D coordinates of the 23 joint marker positions, are given as inputs to the MRD model. To ensure that the model finds the correspondence between the two spaces if and only if it exists, the dimensionality of the latent space (X) is set to the sum of the dimensionality of the original spaces, i.e. $8+23=31$, in spite of the fact that the dimensionality of the latent space (X) could be much lower because of the inherent correlation that exists in the dataset. The model automatically finds the relevance of every dimension in latent space (X) using the ARD procedure by assigning higher ARD weights to relevant dimensions, and making it close to zero when there is little relevance, as such high dimensionality of the latent space, in the beginning, will not be a problem either.

Fig. 4a shows the scaled ARD weights for all 31 dimensions of the latent space (X) obtained using the MRD model. The threshold (δ) is set to 0.04 as shown by the dotted black line, leads to six significant dimensions {1,2,9,10,11,12,13 and 14} which are considered for further investigations. The value of this threshold (δ) is specific for each subject, mostly near to zero, and decided in such a way that a latent dimension which contributes to the reconstruction of higher dimensional spaces should not be left out of the further analysis. Dimensions $\{1$ and $2\}$ represents the subspace (X^y), which is private to sEMG space and dimensions {9,10,11,12,13 and 14} represents the shared subspace (X^{yz}) between sEMG and the finger kinematics, while dimensions representing the subspace private to finger kinematics (X^z), can rarely be seen, which is a consistent trend across all subjects.

A dimension in latent space (X) represents either only a muscle synergy, or only a kinematic synergy, or a coupling of both synergies. Encoded information in a latent dimension related to sEMG or finger kinematics can be understood by sampling new latent points (X_{samp}) along a dimension, and mapping them to the related higher dimensional spaces by calculating the likelihood $P(Y|X_{samp})$ or $P(Z|X_{samp})$.

1) Muscle Synergies Independent of Kinematic synergies: Latent dimensions $\{1$ and $2\}$ represent the muscle synergies that are independent of finger kinematics. Fig. 4b shows the projection of the latent space into dimension $\{1$, and $2\}$. The red dots in Fig. 4b corresponds to the posterior mean of each training data points projected onto a 2D space, while the gradient of the background corresponds to the posterior variance (white for low variance and black for high variance).

Encoded muscle activation values in the dimension $\{1\}$ are obtained by sampling the latent points along with it (the dotted blue line), while keeping the values fixed corresponding to other latent dimensions. Visualization of muscle activation values corresponding to three latent points, indicated by the blue arrow in Fig. 4b, are shown in Fig. 4c. Blue bars shows the minimum activation values while yellow bars on the top of blue bars indicate the amount of modulation in the activation values when moving from left to right in Fig. 4b. Similarly,

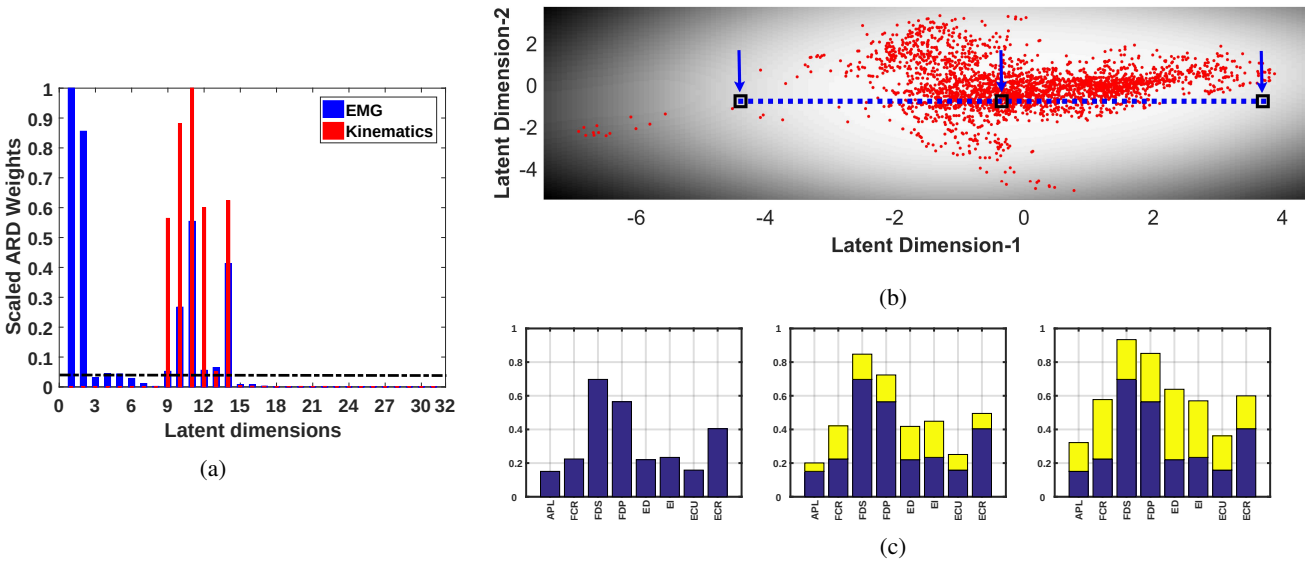

Fig. 4: The shared latent space (X) obtained using the MRD model and the sample investigation process to find encoded information in the latent dimensions, (a) shows the scaled ARD weights corresponding to every latent dimension in X. Dimensions $\{1, 2\}$ represents the subspace, private to sEMG (X^y), while dimensions $\{9, 10, 11, 12, 13$ and $14\}$ represents the shared subspace (X^{yz}) between sEMG and the finger kinematics, (b) shows the projection of latent space into dimensions $\{1$ and $2\}$, and a sample process to find the encoded information in a latent dimension. Muscle activation values corresponding to dimension $\{1\}$ can be obtained by sampling the latent points along it as shown by the dotted blue line, while keeping the points fixed on the other dimensions. Visualization of muscle activation values corresponding to the three latent points, indicated by the blue arrow, are shown in (c). Blue bars shows the minimum activation values while yellow bars on the top of blue bars indicate the amount of modulation in the activation values when moving from left to right in (b).

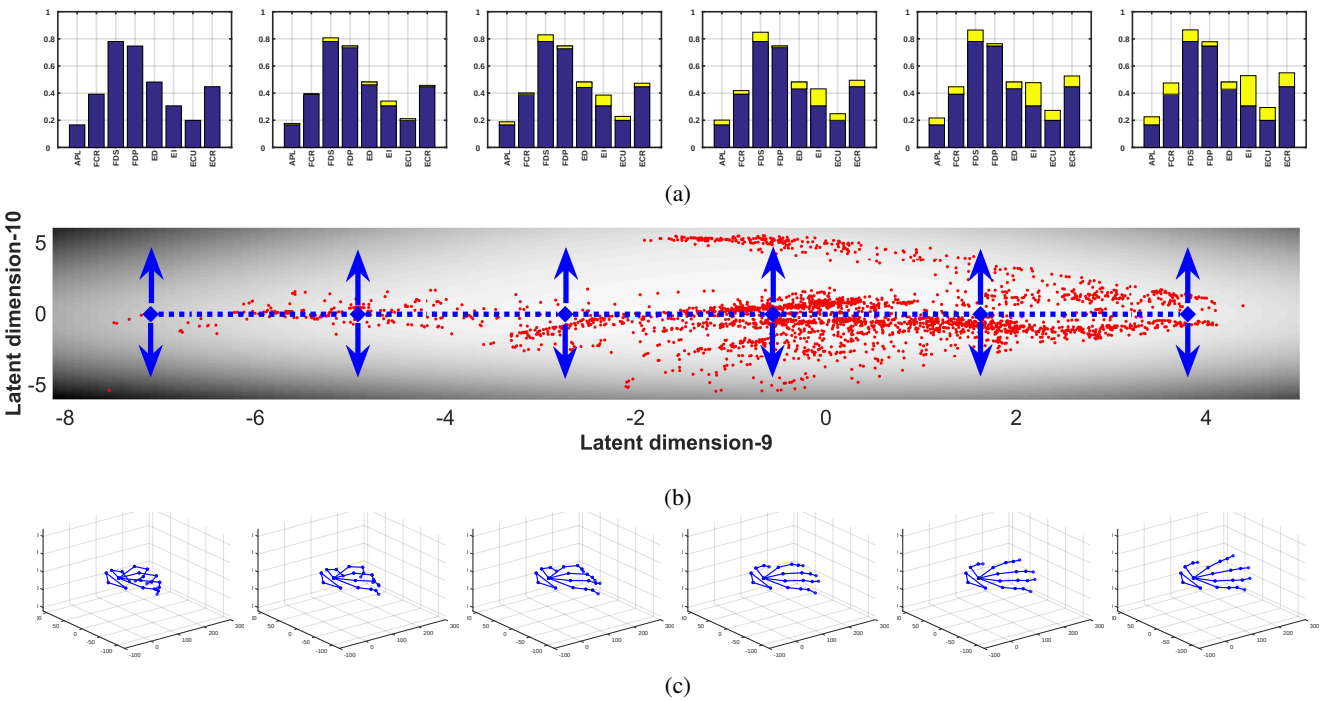

Fig. 5: Exploration of couped latent dimension in the shared latent space (X), (b) shows the projection of latent space (X) into dimensions $\{9, 10\}$. When sampling the latent points along the dimension $\{9\}$ as shown by the dotted blue line, proportional and simultaneous estimation of flexion and extension of all fingers along with related muscle activations is achieved. The visualization of muscle activations and finger kinematics corresponding to the six latent points, indicated by the blue arrow, are shown in (a) and (c), respectively. Blue bars shows the minimum activation values while yellow bars on the top of blue bars indicate the amount of modulation in the activation values when moving along the latent dimension $\{9\}$.

the activation values corresponding to the latent dimension $\{2\}$ can also achieved.

However, the presence of second latent dimension private to sEMG space was not consistent across the subject and have not been considered for further analysis. When moving along these independent latent dimensions from left to right as shown in Fig. 4c, muscle activations, corresponding to all the muscles, increase continuously. Monotonically increasing activation values for all the muscles indicate that these latent dimensions capture the overall variance of the sEMG data, instead of any task-specific variability. A video demonstration (Independent_LD.mp4) of change in activation values when moving along the independent latent dimension is provided in the supplementary material.

2) Muscle Synergies associated with Kinematic Synergies: Dimensions $\{$9,10,11,12,13 and 14$\}$ represent the muscle synergies which are associated with kinematic synergies and referred as coupled latent dimensions, in this study. This association can be understood by the same procedure of sampling the latent points along one of the coupled latent dimension at a time and correlating it with both, the muscle activations and finger kinematics as shown in Fig. 5.

Fig. 5b shows the projection of latent space into dimensions $\{$9 and 10$\}$. The dotted blue line in Fig. 5b represents that the latent points are being sampled along the dimension $\{9\}$. The sampled latent points X_{samp} are mapped back to both the observational spaces by calculating the likelihoods $P(Y|X_{samp})$ and $P(Z|X_{samp})$. Reconstructed finger kinematics motion resemble with the all finger flexion-extension task. Visualization of the reconstructed muscle activation values and the corresponding finger kinematics at those six latent points which are indicated by the blue arrow in Fig. 5b are shown in Fig. 5a and 5c, respectively. Again the Blue bars in 5a indicate the minimum activation values while yellow bars on the top of blue bars indicate the amount of modulation in the activation values when moving from left to right in Fig. 5b . Recovered finger motions corresponding to these coupled latent dimensions for all the subjects is presented in Table III while the muscle activation values for subject 1 (S1) are shown in Fig. 6.

Muscle activation values represented by coupled latent dimensions do not follow the trend of those represented by independent latent dimensions. In fact, moving along a coupled latent dimension, when resulting in the increase of activation values for some muscles, it results in the increase or decrease or no change in the activation values corresponding to other muscles, and these variations are specific to a coupled latent dimension. This gives a notion that a coupled latent dimension encodes those activation values which are desired to achieve the finger kinematics represented by it. A video demonstration (Coupled_LD.mp4) of the generated muscle activations and related finger kinematics, when moving along the coupled latent dimensions are provided in the supplementary material.

It could be argued that the muscle synergy represented by a coupled latent dimension could be capturing the task-specific variability for a subject in contrast to the independent muscle synergy (dim. $\{1\}$) which is capturing the overall variance of the sEMG data. As coupled synergies are responsible for generating only a subset of values rather than large range of activation values (overall variance of the input sEMG), justifies the lower values of the ARD weights for the coupled muscle synergies (comparatively smaller blue bars for the dimensions 9,10,11,12,13, and 14) when compared with the higher ARD weight of an independent muscle synergy (blue bar for the dimension -1). A similar trend has also been observed in the remaining subjects.

B. Kinematic Estimation

The MRD model facilitates a way to interpret how different but related observation spaces interact with each other, by finding a shared latent space (X). In this study, the coupled latent dimensions represent the association of muscle activation with finger kinematics in the low dimensional space. The shared latent space provides us with a platform to visualize in the kinematic space, from what can be seen in the sEMG space within a fully probabilistic framework. Hence, the predicted point in the kinematic space gives a distribution instead of a point estimation, which makes the entire prediction process robust [44]. The finger kinematics is estimated from the shared latent space (X) by following the procedure presented in Algorithm 1.

Quality of the estimated finger kinematics using the proposed and other commonly used regression approaches have been evaluated on three metrics namely RMSE, R-square, and the Correlation Coefficient (ρ) as shown in Table IV. The estimated marker positions follow the measured values with an average correlation of 0.91 ± 0.03, R-square of 0.84 ± 0.05 and the RMSE of 3.44 ± 0.87, respectively, which show the best results when compared with other regression methods. Subject wise RMSE corresponding to all the five methods have been shown in Fig. 7.

Fig. 8 shows that the proposed method has significantly outperformed ($p \leq 0.0001$) other traditional regression approaches, evaluated using pair-wise t-tests following the result of repeated measure one-way ANOVA.

VI. Discussion

This paper showed that there exists an association between finger kinematics and muscle activations, manifested in the coupled latent dimensions, by jointly studying the two related spaces through multi-view learning. This study also demonstrated how the proportional and simultaneous estimation of finger kinematics can be achieved by making use of the shared variance between the Muscle Activation space (Y) and the Kinematic space (Z) in a probabilistic framework.

A. Nonlinear Kinematic Synergies

Table III shows the reconstructed finger kinematics when the dimensions representing kinematic synergies in the shared latent space (X) were explored. Dimension 9 consistently encodes the kinematic information of the All Finger Flexion-Extension (AFFE) task even across different subjects. This can be attributed that dimension 9 captures a larger variance of kinematic data from this task, nearly 20 markers' positions

TABLE III: Encoded finger kinematics in latent dimensions for 10 subjects

	9	10	11	12	13	14	15
Subject 1	AFFE	Middle	Ring	Index	Thumb	Thumb	—-
Subject 2	AFFE	Ring+Little	Thumb	Middle+Ring+Thumb	Index	—-	—-
Subject 3	AFFE	Ring+Little	Middle	Thumb+Index	Middle+Ring	—-	Thumb
Subject 4	AFFE	Middle+Ring	Ring+Little+Thumb	Thumb	Thumb+Index	—-	–
Subject 5	AFFE	—-	Middle	Ring	Thumb,Index	—-	Thumb
Subject 6	AFFE	Thumb	Middle+Ring+Little+Thumb	Little	—-	Ring	—-
Subject 7	AFFE	Ring+Little	Middle	Index	—-	—-	—-
Subject 8	AFFE	Ring+Little	Thumb	Middle	—-	—-	—-
Subject 9	AFFE	Thumb+Little	Index+Middle+Ring+Little	Thumb+Index	Thumb+Index	Index+Ring	—-
Subject 10	AFFE	Thumb	Index	Middle	Little	——	—-

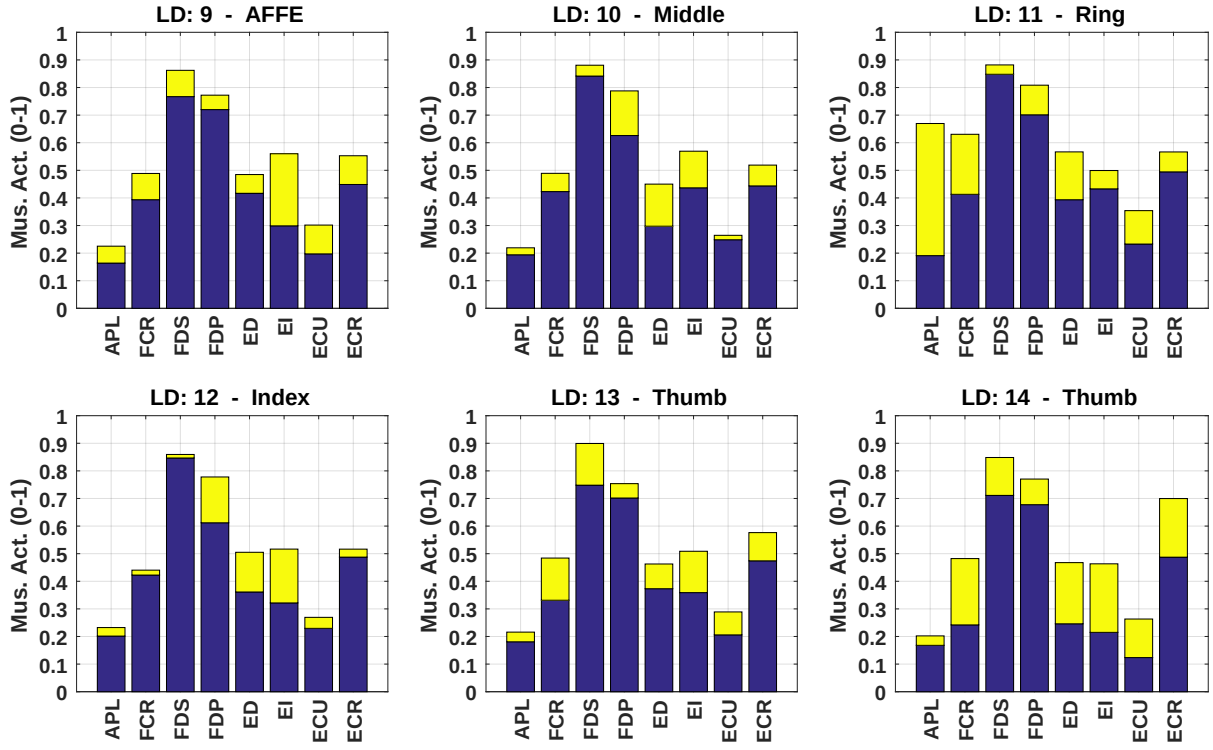

Fig. 6: Shows the muscle activation values encoded in the shared latent dimensions {9,10,11,12,13, and 14} . Muscle activation values are obtained by following the same procedure of sampling latent points along a dimension. Blue bars shows the minimum activation values while yellow bars on the top of the blue bars indicate the amount of modulation in the activation values when moving along the dimension.

varying as compared to only 5 to 6 markers' position changing at a time in the Individual Finger Flexion-Extension (IFFE) task.

The kinematics of the thumb, on the other hand, is encoded in a separate dimension. This highly independent motion of the thumb is captured in most of the subjects (8 out of 10). While, coupled motion of the thumb with other fingers is captured in the other dimensions. From the kinematics point of view, this is likely due to the opposite direction of the thumb as compared with motions of the other fingers. The thumb also has more degrees-of-freedom (DOFs) and has more independent movements compared to the rest of the other fingers.

The kinematics of the individual finger's movement are inconsistently encoded in different dimensions 10-13 across subjects. Some dimensions contain only the data variance of individual finger exclusively, while others contain the variance of individual finger movements coupled with other finger's movements. This natural coupling of finger movements is also summarized in Table III, which describes the anatomical and kinesiological similarities of the targeted muscles to control similar fingers. The synergies obtained by our method captures these anatomical couplings quite well, with couplings that occur between adjacent fingers, for example Index-Middle-Ring, rather than with distant fingers Index-Little. These result consistently showed that the extracted muscle synergies are congruent with the hand physiology.

The finger kinematics and the sEMG signals are highly non-

TABLE IV: The mean RMSE, Correlation Coefficient (ρ) and R-Square calculated between the estimated and original finger kinematics along with time required to predict a sample point.

Regression Methods	RMSE	Correlation coefficient(ρ)	R-Square	Time (in milliseconds)
LR using Reduced Dimension (LR-RD)	8.08± 1.28	0.50±0.08	0.31±0.13	0.000,09±0.000,1
LR using Full Dimension (LR-Full)	7.66±1.22	0.57±0.07	0.38±0.12	0.000,43±0.000,10
ANN using Reduced Dimension (ANN-RD)	6.64±1.19	0.68±0.04	0.46±0.10	0.06±0.002
ANN using Full Dimension (ANN-Full)	5.07 ± 0.90	0.82 ±0.04	0.68±0.07	0.09±0.010
Proposed Method	**3.4±0.89**	**0.91 ± 0.03**	**0.84± 0.05**	2.6 ± 0.79

LR- Linear Regression, ANN - Artificial Neural Network.

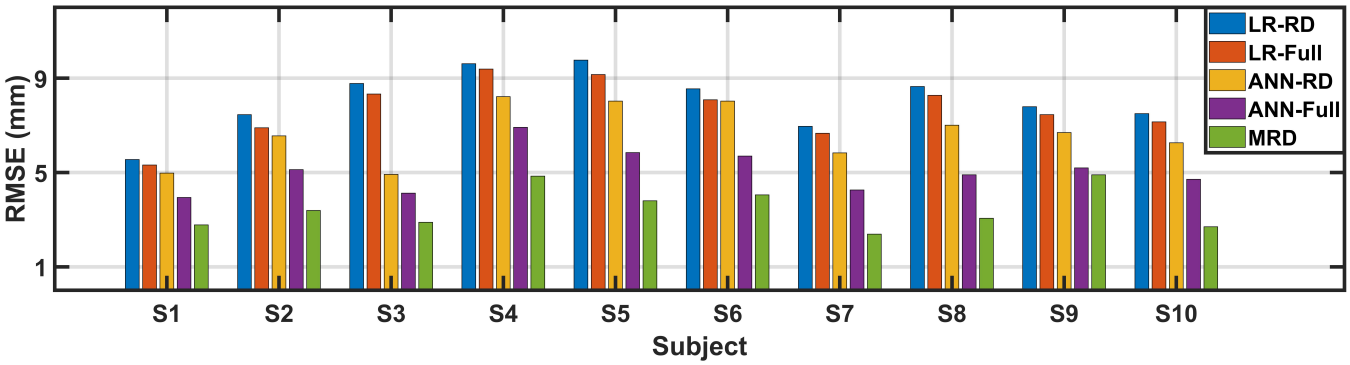

Fig. 7: Root Mean Square Error (RMSE) calculated between the measured and estimated 3D coordinate corresponding to 23 marker positions in the hand for all 10 subjects corresponding to all the five methods

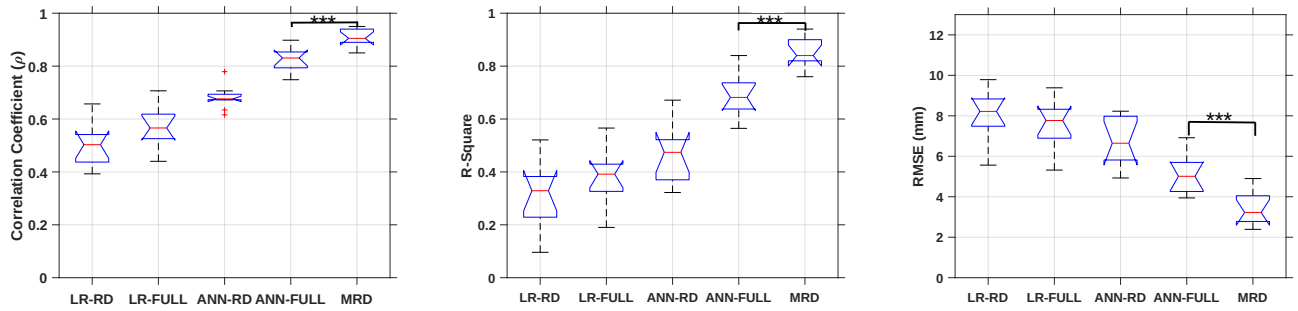

(a) (b) (c)

Fig. 8: Comparison of estimation performance between MRD and other commonly used regression approaches. Evaluation on three metrics: (a) Correlation (b) R-square and (c) Root Mean Square Error (RMSE). *** indicates p $\leq$ 0.0001

linear in nature, and therefore an algorithm that can cope with nonlinearities is better suited for their analysis. Thus extracting nonlinear muscle and kinematic synergies, using the MRD model, and its effectiveness in reconstructing the related higher dimensional spaces and accurately predicting finger kinematics justifies its use. From the best of our knowledge, this is the first sEMG study to introduce a factorized latent model to nonlinearly extract the muscle and kinematic synergies with relevant weights associated with each synergy, which explains its importance in the related spaces.

B. Estimation of Finger Kinematics

The experimental results in the previous section show that the MRD model with the automatic dimensionality determination of the latent spaces is an effective model for learning the correlations that exist between the muscle activations and the finger kinematics. Although the dimensions are highly redundant in the kinematic space, the proposed model is able to reconstruct back as large as 69 dimensions $(23 \times 3 = 69)$ on the hand skeleton model.

The choice of operating in the output joint marker space was to induce high dimensionality in the output space and to show that the model is capable of dealing with high dimensional data very well. One other advantage of the proposed method is that it can learn corresponding latent space manifolds from any data representation or output spaces, such as joint velocity or joint torque and stiffness space [45]. Operating in these spaces is particularly useful since these can be explicitly used as direct control signals for robotic devices.

One advantage of using the proposed shared synergistic model is its ability to consider nonlinear mappings using GPs with an ARD covariance function shown in (5). This gives a data-driven approach to address the compact representation of

both the sEMG and high-DOF finger kinematics.

C. Implementation and limitations

This study is limited to offline analysis with data from healthy and able-bodied subjects to test the feasibility of our approach. Also, in this study, the optimization of the parameters of the muscle activation model (Section IV-B) was pre-trained using all the data available per subject, although the model parameters acquired on the training data only are to be investigated for the validation dataset. Though this can be used as an initial benchmark, for future implementations, further verification and validation of the proposed approach has to be done for the online applicability by training different models using data from amputees and testing them in real-life situations [20].

In practice, it is desirable for the controller to use as little calibration data as possible and should generalize to movements for which exhaustive training data is not available [1]. Most of the computational time (99%) is due to the training of the MRD model. The typical computational complexity of a sparse implementation of the MRD model is $O(Nm^2)$, where N is the number of data sample used, and m is the number of inducing points. This can be quite prohibitive with many sEMG applications where re-calibration is done to adapt to the time-varying nature of sEMG.

VII. Conclusion and Future Work

Toward intuitive control of multi-fingered prosthesis, this paper has introduced and evaluated the use of Manifold Relevance Determination (MRD), a multi-view learning model with a nonparametric Bayesian approach.

We have found that there exist an association between the nonlinear muscle and kinematic synergies, and the finger-kinematics estimation from muscle activations using the acquired synergies outperformed other commonly used linear and nonlinear regression approaches. As a conclusion, the findings of this study not only presents a viable solution for accurate and intuitive myoelectric control for handling high DOFs in robotic hand prosthesis but also provides a new perspective on the muscle synergies in the motor control community.

For future work, the same approach can be used to understand the neural implementation of muscle synergies by simultaneously recording neural and muscle activities when performing different motor tasks [46]. The existence of the shared part in the latent space supports the muscle synergy hypothesis and the method for extracting muscle synergies from sEMG signals. This work can be further extended by including task-related variables for understanding the relationship among these three different but related observational spaces. Along with this, the online application of our framework to a real multi-fingered hand is also our essential future work.

Acknowledgment

This work was supported by the Grant-in-Aid for Scientific Research from Japan Society for the Promotion of Science (No. 16H06534). We would also like to thank Vishal Gaurav and Dr. Nishanth Koganti for their invaluable insights and general support.

References

[1] J. Hahne, F. Biebmann, N. Jiang, H. Rehbaum, D. Farina, F. Meinecke, K.-R. Muller, and L. Parra, "Linear and nonlinear regression techniques for simultaneous and proportional myoelectric control," *IEEE Trans. on Neural Syst. and Rehabil. Eng.*, vol. 22, no. 2, pp. 269–279, March 2014.

[2] D. Farina, N. Jiang, H. Rehbaum, A. Holobar, B. Graimann, H. Dietl, and O. Aszmann, "The extraction of neural information from the surface EMG for the control of upper-limb prostheses: Emerging avenues and challenges," *IEEE Trans. on Neural Syst. and Rehabil. Eng.*, vol. 22, no. 4, pp. 797–809, 2014.

[3] Y. Huang, K. B. Englehart, B. Hudgins, and A. D. Chan, "A gaussian mixture model based classification scheme for myoelectric control of powered upper limb prostheses," *IEEE Trans. on Biomedical Eng.*, vol. 52, no. 11, pp. 1801–1811, 2005.

[4] A. J. Young, L. H. Smith, E. J. Rouse, and L. J. Hargrove, "Classification of simultaneous movements using surface EMG pattern recognition," *IEEE Trans. on Biomedical Eng.*, vol. 60, pp. 1250–1258, 2013.

[5] N. Jiang, H. Rehbaum, I. Vujaklija, B. Graimann, and D. Farina, "Intuitive, online, simultaneous, and proportional myoelectric control over two degrees-of-freedom in upper limb amputees," *IEEE Trans. on Neural Syst. and Rehabil. Eng.*, vol. 22, no. 3, pp. 501–510, 2014.

[6] M. Ison and P. Artemiadis, "The role of muscle synergies in myoelectric control: trends and challenges for simultaneous multifunction control," *Journal of Neural Engineering*, vol. 11, no. 5, p. 051001, 2014.

[7] N. Jiang, S. Dosen, K.-R. Müller, and D. Farina, "Myoelectric control of artificial limbs–is there a need to change focus," *IEEE Signal Process. Mag*, vol. 29, no. 5, pp. 152–150, 2012.

[8] V. Kumar, Y. Tassa, T. Erez, and E. Todorov, "Real-time behaviour synthesis for dynamic hand-manipulation," in *IEEE Int. Conf. on Robotics and Automation (ICRA)*. IEEE, 2014, pp. 6808–6815.

[9] M. Barsotti, S. Dupan, I. Vujaklija, S. Došen, A. Frisoli, and D. Farina, "Online finger control using high-density emg and minimal training data for robotic applications," *IEEE Robotics and Automation Letters*, vol. 4, no. 2, pp. 217–223, 2018.

[10] A. d'Avella, P. Saltiel, and E. Bizzi, "Combinations of muscle synergies in the construction of a natural motor behavior," *Nature neuroscience*, vol. 6, no. 3, pp. 300–308, 2003.

[11] J. Romero, T. Feix, C. H. Ek, H. Kjellstrom, and D. Kragic, "Extracting postural synergies for robotic grasping," *IEEE Trans. on Robotics*, vol. 29, no. 6, pp. 1342–1352, 2013.

[12] A. Damianou, C. Ek, M. Titsias, and N. Lawrence, "Manifold relevance determination," *arXiv preprint arXiv:1206.4610*, 2012.

[13] I. V. Grinyagin, E. V. Biryukova, and M. A. Maier, "Kinematic and dynamic synergies of human precision-grip movements," *Journal of neurophysiology*, vol. 94, no. 4, pp. 2284–2294, 2005.

[14] M. Santello, M. Flanders, and J. F. Soechting, "Postural hand synergies for tool use," *The Journal of Neuroscience*, vol. 18, no. 23, pp. 10 105–10 115, 1998.

[15] A. d'Avella, A. Portone, L. Fernandez, and F. Lacquaniti, "Control of fast-reaching movements by muscle synergy combinations," *The Journal of neuroscience*, vol. 26, no. 30, pp. 7791–7810, 2006.

[16] L. H. Ting, "Dimensional reduction in sensorimotor systems: a framework for understanding muscle coordination of posture," *Progress in brain research*, vol. 165, pp. 299–321, 2007.

[17] M. Tagliabue, A. Ciancio, T. Brochier, S. Eskiizmirliler, and M. Maier, "Differences between kinematic synergies and muscle synergies during two-digit grasping," *Frontiers in human neuroscience*, vol. 9, 2015.

[18] N. Jiang, K. B. Englehart, and P. A. Parker, "Extracting simultaneous and proportional neural control information for multiple-dof prostheses from the surface electromyographic signal," *IEEE Transactions on Biomedical Eng.*, vol. 56, no. 4, pp. 1070–1080, 2009.

[19] P. K. Artemiadis and K. J. Kyriakopoulos, "Emg-based control of a robot arm using low-dimensional embeddings," *IEEE Transactions on Robotics*, vol. 26, no. 2, pp. 393–398, 2010.

[20] N. Jiang, I. Vujaklija, H. Rehbaum, B. Graimann, and D. Farina, "Is accurate mapping of EMG signals on kinematics needed for precise online myoelectric control?" *IEEE Trans. on Neural Syst. and Rehabil. Eng.*, vol. 22, no. 3, pp. 549–558, May 2014.

[21] J. Ma, N. V. Thakor, and F. Matsuno, "Hand and wrist movement control of myoelectric prosthesis based on synergy," *IEEE Transactions on Human-Machine Systems*, vol. 45, no. 1, pp. 74–83, 2015.

[22] S. Zhang, X. Zhang, S. Cao, X. Gao, X. Chen, and P. Zhou, "Myoelectric pattern recognition based on muscle synergies for simultaneous control of dexterous finger movements," *IEEE Transactions on Human-Machine Systems*, vol. 47, no. 4, pp. 576–582, 2017.

[23] C. Lin, B. Wang, N. Jiang, and D. Farina, "Robust extraction of basis functions for simultaneous and proportional myoelectric control via sparse non-negative matrix factorization," *Journal of neural engineering*, 2017.

[24] S. Muceli, N. Jiang, and D. Farina, "Extracting signals robust to electrode number and shift for online simultaneous and proportional myoelectric control by factorization algorithms," *IEEE Trans. on Neural Syst. and Rehabil. Eng.*, vol. 22, no. 3, pp. 623–633, 2014.

[25] C. Alessandro, I. Delis, F. Nori, S. Panzeri, and B. Berret, "Muscle synergies in neuroscience and robotics: from input-space to task-space perspectives," *Frontiers in computational neuroscience*, vol. 7, p. 43, 2013.

[26] S. A. Chvatal, G. Torres-Oviedo, S. A. Safavynia, and L. H. Ting, "Common muscle synergies for control of center of mass and force in nonstepping and stepping postural behaviors," *Journal of neurophysiology*, vol. 106, no. 2, pp. 999–1015, 2011.

[27] L. H. Ting and J. M. Macpherson, "A limited set of muscle synergies for force control during a postural task," *Journal of neurophysiology*, vol. 93, no. 1, pp. 609–613, 2005.

[28] M. Spüler, N. Irastorza-Landa, A. Sarasola-Sanz, and A. Ramos-Murguialday, "Extracting muscle synergy patterns from emg data using autoencoders," in *International Conference on Artificial Neural Networks*. Springer, 2016, pp. 47–54.

[29] I. Delis, B. Berret, T. Pozzo, and S. Panzeri, "Quantitative evaluation of muscle synergy models: a single-trial task decoding approach," *Frontiers in computational neuroscience*, vol. 7, p. 8, 2013.

[30] M. Santello, M. Bianchi, M. Gabiccini, E. Ricciardi, G. Salvietti, D. Prattichizzo, M. Ernst, A. Moscatelli, H. Jörntell, A. M. Kappers *et al.*, "Hand synergies: integration of robotics and neuroscience for understanding the control of biological and artificial hands," *Physics of life reviews*, vol. 17, pp. 1–23, 2016.

[31] J. Ngeo, T. Tamei, K. Ikeda, and T. Shibata, "Modeling dynamic high-dof finger postures from surface emg using nonlinear synergies in latent space representation," in *2015 37th Annual International Conference of the IEEE Engineering in Medicine and Biology Society (EMBC)*. IEEE, 2015, pp. 2095–2098.

[32] A. C. Damianou, M. K. Titsias, and N. D. Lawrence, "Variational inference for uncertainty on the inputs of gaussian process models," *arXiv preprint arXiv:1409.2287*, 2014.

[33] N. Lawrence, "Probabilistic non-linear principal component analysis with gaussian process latent variable models," *The Journal of Machine Learning Research*, vol. 6, pp. 1783–1816, 2005.

[34] M. K. Titsias and N. D. Lawrence, "Bayesian gaussian process latent variable model," in *International Conference on Artificial Intelligence and Statistics*, 2010, pp. 844–851.

[35] A. Damianou, M. K. Titsias, and N. D. Lawrence, "Variational gaussian process dynamical systems," in *Advances in Neural Information Processing Systems*, 2011, pp. 2510–2518.

[36] A. Damianou, M. K. Titsias, and N. Lawrence. Vargplvm software for matlab and r. [Online]. Available: https://github.com/SheffieldML/vargplvm

[37] N. Pratt, "Anatomy and kinesiology of the hand," *Rehabilitation of the Hand and Upper Extremity. 6th ed. Philadelphia: Elsevier*, pp. 1–17, 2011.

[38] I. Carpinella, P. Mazzoleni, M. Rabuffetti, R. Thorsen, and M. Ferrarin, "Experimental protocol for the kinematic analysis of the hand: definition and repeatability," *Gait & Posture*, vol. 23, no. 4, pp. 445–454, 2006.

[39] T. S. Buchanan, D. G. Lloyd, K. Manal, and T. F. Besier, "Neuromusculoskeletal modeling: estimation of muscle forces and joint moments and movements from measurements of neural command," *Journal of applied biomechanics*, vol. 20, no. 4, p. 367, 2004.

[40] K. Manal, R. V. Gonzalez, D. G. Lloyd, and T. S. Buchanan, "A real-time EMG-driven virtual arm," *Computers in biology and medicine*, vol. 32, no. 1, pp. 25–36, 2002.

[41] T. Tamei and T. Shibata, "Fast reinforcement learning for three-dimensional kinetic human–robot cooperation with an EMG-to-activation model," *Advanced Robotics*, vol. 25, no. 5, pp. 563–580, 2011.

[42] J. G. Ngeo, T. Tamei, and T. Shibata, "Continuous and simultaneous estimation of finger kinematics using inputs from an EMG-to-muscle activation model," *J Neuroeng Rehabil*, vol. 11, no. 122, pp. 3–11, 2014.

[43] N. Jiang, J. L. Vest-Nielsen, S. Muceli, and D. Farina, "Emg-based simultaneous and proportional estimation of wrist/hand kinematics in uni-lateral trans-radial amputees," *Journal of neuroengineering and rehabilitation*, vol. 9, no. 1, p. 42, 2012.

[44] P. Trautman, "Manifold relevance determination: Learning the latent space of robotics," *arXiv preprint arXiv:1705.03158*, 2017.

[45] D. Shin, J. Kim, and Y. Koike, "A myokinetic arm model for estimating joint torque and stiffness from EMG signals during maintained posture," *Journal of neurophysiology*, vol. 101, no. 1, pp. 387–401, 2009.

[46] C. B. Hart and S. F. Giszter, "A neural basis for motor primitives in the spinal cord," *Journal of Neuroscience*, vol. 30, no. 4, pp. 1322–1336, 2010.